STUDIES ON THE PROCESSING AND PROPERTIES OF CONDUCTIVE SINGLE FILLERS AND HYBRID FILLERS FILLED SILICONE ELASTOMER COMPOSITES

by

KENNETH KONG THEAN SOON

Thesis submitted in fulfillment of the requirements
for the degree of
Master of Science

February 2012

DECLARATION

I declare that the contents presented in this thesis are my own original research work which was done in Universiti Sains Malaysia, Malaysia and Queen Mary University of London, United Kingdom. Wherever contributions of others are involved, every effort is made to indicate this clearly, with due reference to literature, and acknowledgement of collaborative research and discussions. This thesis has not been submitted for any other degree.

Signature :

Name : Kenneth Kong Thean Soon

Date : 14th February 2012

In my capacity as main supervisor of the candidate's thesis, I certify that the above statements are true to the best of my knowledge.

Signature :

Name : Associate Professor Dr. Mariatti Jaafar @ Mustapha

Date : 14th February 2012

ACKNOWLEDGEMENTS

Firstly, I would like to assert my sincerest and deepest gratitude to my supervisor, Associate Professor Dr. Mariatti Jaafar @ Mustapha for her valuable guidance, wealth of knowledge, and unwavering support provided to me throughout the duration of my MSc. study. I would also like to thank my co-supervisor, Associate Professor Dr. Azura Rashid and the Dean of School of Materials Science and Mineral Resources Engineering (SMMRE), Professor Ahmad Fauzi b. Mohd Noor for the unflinching advices, encouragement, and moral support given to me. Without the three of them, this study would not have been successful.

I acknowledge Universiti Sains Malaysia for the financial support given to me through the Universiti Sains Malaysia-Research University-Postgraduate Research Grant Scheme (USM-RU-PRGS) and USM Fellowship. The USM-RU-PRGS covers any expenses related to the research project while the USM Fellowship covers the tuition fees, examination fees, and monthly living allowance.

I am extremely fortunate to have the opportunity to be in Queen Mary University of London (QMUL), United Kingdom for a short research attachment under the British Council's Prime Minister Initiative 2 (PMI-2) Research Grant. This opportunity would not have come without the help and support of Dr. Mariatti, Dr. Azura, British Council, and QMUL. In QMUL, I was placed in the Rubber Research Group under the supervision of Dr. James J. C. Busfield. I gratefully thank Dr. James and Professor Alan G. Thomas for their advices, supervision, encouragement, and words of wisdom and inspiration. Not to forget, many thanks to the members of

Rubber Research Group, especially Dr. Philip Gabriel for helping me to settle down when I was in London.

I would also like to acknowledge the technical advices and assistance given by the staffs of SMMRE and QMUL. The staffs of SMMRE are Mrs. Fong Lee Lee, Mr. Gnanasegaran a/l N. B. Dorai, En. Mohd Faizal b. Mohd Kassim, En. Shahril Amir b. Saleh, En. Mohammad b. Hassan, En. Shahrul Ami b. Zainal Abidin, En. Mohd. Suhaimi b. Sulong, En. Abdul Rashid b. Selamat, En. Mohd Azam b. Rejab, and En. Muhammad Khairi b. Khalid. The staffs of QMUL are Dr. Zofia Luklinska, Dr. Nima Roohpour, Dr. Emilliano Billoti, Mr. Mick Willis, Mr. John Caulfield, and Mr. Christopher Reynolds.

Special thanks dedicated to Suriatti bt. Ghazali, Norkhairunnisa bt. Mazlan, and Chua Tze Ping, who have guided me and provided me assistance in my laboratory and experimental work. They also shared their experiences and advices that are useful for my research and thesis writing. Not to forget, the group of postgraduate friends and my girlfriend, Kong Siew Mui, who gave their endless support and have been a great company throughout the duration of my MSc. study.

Last but certainly not least, I humbly thank my family members; especially my parents who showered me with love and had tirelessly supported me morally and financially until I complete my MSc. study.

TABLE OF CONTENTS

DECLARATION		ii
ACKNOWLEDGEMENT		iii
TABLE OF CONTENTS		v
LIST OF TABLES		x
LIST OF FIGURES		xii
LIST OF ABBREVIATIONS		xvii
LIST OF SYMBOLS		xix
LIST OF APPENDICES		xx
ABSTRAK		xxi
ABSTRACT		xxii
CHAPTER 1 – INTRODUCTION		
1.1	Introduction	1
1.2	Problem Statement	4
1.3	Research Objectives	6
1.4	Organization of Thesis	6
CHAPTER 2 – LITERATURE REVIEW		
2.1	History and Chemistry of Silicone	8
	2.1.1 Silicone Elastomers	11
	2.1.2 Polydimethylsiloxane	12
2.2	Curing System of Silicone Elastomers	13
	2.2.1 RTV-1 Condensation Curing	14
	2.2.2 RTV-2 Condensation Curing	16
	2.2.3 Addition Curing	17

2.2.4 Free Radical Curing 18
2.3 Introduction to Carbon 19
2.4 Carbon Nanotubes 22
2.4.1 Single-walled Carbon Nanotubes 24
2.4.2 Multi-walled Carbon Nanotubes 26
2.4.3 Synthesis and Production of Carbon Nanotubes 28
2.4.3.1 Carbon Arc Discharge 28
2.4.3.2 Laser Ablation Technique 30
2.4.3.3 Chemical Vapor Deposition 30
2.4.4 Functionalization of Carbon Nanotubes 31
2.4.4.1 Acid Treatment 32
2.4.4.2 Amine Functionalization 33
2.4.4.3 Amino Functionalization 34
2.5 Graphite 35
2.5.1 Graphite Oxide 36
2.5.2 Graphite Intercalation Compounds 36
2.5.3 Expanded Graphite and Graphite Nanoplatelets 37
2.5.4 Synthesis of Graphite Nanoplatelets 38
2.6 Polymer/CNT and Polymer GNP Composites 40
2.6.1 Processing of Polymer Composites 40
2.6.1.1 Solution Processing 41
2.6.1.2 Melt Processing 42
2.6.1.3 *In Situ* Polymerization 43
2.6.2 Properties of Polymer/CNT and Polymer/xGnP Composites 44
2.6.2.1 Thermal Properties 44
2.6.2.2 Mechanical Properties 47
2.6.2.3 Electrical Conductivity 48

2.7 Polymer/Hybrid Fillers Composites 51

CHAPTER 3 – MATERIALS AND METHODOLOGY

3.1 Materials and Chemicals 53

3.1.1 Polydimethysiloxane 53

3.1.2 Pristine Multi-walled Carbon Nanotubes 54

3.1.3 Hydroxyl Functionalized Multi-walled Carbon Nanotubes 54

3.1.4 Carboxyl Functionalized Multi-walled Carbon Nanotubes 55

3.1.5 Exfoliated Graphite Nanoplatelets 55

3.1.6 Toluene 56

3.2 Experimental Methods 57

3.2.1 Research Overview 57

3.2.2 Characterization of Raw Materials 58

3.2.2.1 Surface Morphology of Fillers 58

3.2.2.2 Fourier Transform Infrared Spectroscopy 60

3.2.2.3 Raman Spectroscopy 60

3.2.2.4 Elemental Analysis of Fillers 60

3.2.3 Fabrication of Composites 61

3.2.3.1 Fabrication of PDMS/MWCNT-p via Solution Mixing (Stage 1) 61

3.2.3.2 Fabrication of PDMS/MWCNT-p via Mini-extruder Method (Stage 1) 64

3.2.3.3 Fabrication of PDMS/Functionalized MWCNT and PDMS/xGnP via Solution Mixing (Stage 2) 66

3.2.3.4 Fabrication of PDMS/Hybrid Fillers via Solution Mixing (Stage 3) 66

3.2.4 Characterization of Composites 67
3.2.4.1 Crosslink Density 67
3.2.4.2 Thermal Conductivity 68
3.2.4.3 Tensile Test 70
3.2.4.4 Fracture Surface Morphology 71
3.2.4.5 Electrical Conductivity Measurement 71
3.2.4.6 Thermogravimetry Analaysis 73
3.2.4.7 Thermomechanical Analysis 74
3.2.4.8 Dynamic Mechanical Analysis 75

CHAPTER 4 – RESULTS AND DISCUSSION

4.1 Introduction 77
4.2 Characterization of Raw Materials 77
4.2.1 Surface Morphology of Fillers 77
4.2.2 Raman Spectroscopy Analysis of MWCNTs 79
4.2.3 Fourier Transform Infrared (FTIR) Spectroscopy Analysis of Fillers 80
4.2.4 Elemental Analysis of Fillers 83
4.2.5 Thermal Stability of Fillers 85
4.3 Effect of Processing Methods on the Properties of PDMS/MWCNT Composites 88
4.3.1 Dispersion and Morphological Study of MWCNTs in PDMS 88
4.3.2 Crosslink Density 94
4.3.3 Thermal Conductivity 95
4.3.4 Tensile Properties 97
4.3.5 Electrical Conductivity 102
4.3.6 Thermal Stability 104
4.3.7 Coefficient of Thermal Expansion 107

4.3.8 Dynamic Mechanical Properties 111

4.4 Properties of PDMS filled with functionalized MWCNTs and PDMS filled with xGnP 115

4.4.1 Dispersion and Morphological Study of fillers in PDMS 115

4.4.2 Crosslink Density 119

4.4.3 Thermal Conductivity 120

4.4.4 Tensile Properties 124

4.4.5 Electrical Conductivity 128

4.4.6 Thermal Stability 131

4.4.7 Coefficient of Thermal Expansion 133

4.4.8 Dynamic Mechanical Properties 136

4.5 Properties of PDMS Hybrid Composites 139

4.5.1 Morphological Study of Hybrid Fillers in PDMS 139

4.5.2 Thermal Conductivity 142

4.5.3 Tensile Properties 144

4.5.4 Electrical Conductivity 147

4.5.5 Thermal Stability 148

4.5.6 Coefficient of Thermal Expansion 150

CHAPTER 5 – CONCLUSIONS AND RECOMMENDATIONS

5.1 Conclusions 153

5.2 Recommendations 155

REFERENCES 157

APPENDICES 172

LIST OF TABLES

		Page
Table 2.1	The basic steps in producing silicone	10
Table 2.2	Comparison of thermal conductivity values of different composite systems	46
Table 2.3	The maximum electrical conductivity achieved for composites filled with different functionalized nanotubes	50
Table 3.1	Typical properties of Sylgard 182 Silicone Elastomer	54
Table 3.2	Typical properties of xGnP® exfoliated graphite nanoplatelets	56
Table 4.1	Composition of elements that are present in MWCNT-p, MWCNT-OH, MWCNT-COOH and xGnP	85
Table 4.2	Thermal stability data for MWCNT-p, MWCNT-OH, MWCNT-COOH, and xGnP, extracted from TGA curves	87
Table 4.3	Crosslink density of composites produced by mini-extruder and solution mixing	94
Table 4.4	Thermal conductivity values of PDMS/MWCNT composites produced by mini-extruder and solution mixing method and the percentage of thermal conductivity improvement	96
Table 4.5	Values of tensile strength, M50, and elongation at break of PDMS composites	98
Table 4.6	Viscosity of PDMS/MWCNTs composite mixture during mixing process	100
Table 4.7	Thermal stability data for PDMS/MWCNT-p composites extracted from TGA curves	106
Table 4.8	Values of T_g and CTE for composites produced by mini-extruder and solution mixing	108
Table 4.9	Values of storage modulus at -130 °C, peak height of tan δ, and the corresponding T_g for composites produced by mini-extruder and solution mixing	112
Table 4.10	Crosslink density for PDMS filled with different MWCNTs and PDMS filled with xGnP	120
Table 4.11	Thermal conductivity values of PDMS filled with different MWCNTs and PDMS filled with xGnP	122
Table 4.12	Thermal stability data for different PDMS composites extracted from TGA curves	133

Table 4.13	T_g and CTE data for different PDMS composites extracted from expansion against temperature curve	134
Table 4.14	Values of storage modulus at -130 °C, peak height of tan δ, and the corresponding T_g for different PDMS composites	138
Table 4.15	Tensile properties of PDMS filled with different ratios of hybrid fillers	145
Table 4.16	Thermal stability data obtained from thermal stability curve of PDMS hybrid composites	149
Table 4.17	T_g and coefficient of thermal expansions data of PDMS hybrid composites	151

LIST OF FIGURES

		Page
Figure 2.1	The basic repeating unit of siloxane, (R_2SiO)	8
Figure 2.2	Chemical formula and structure of trimethylsiloxy-endblocked-polydimethysiloxane	12
Figure 2.3	Summary of curing system and crosslinking reaction for silicone elastomer. The catalyst involved in crosslinking reaction is stated in parentheses.	14
Figure 2.4	Reaction mechanisms in the RTV-1 condensation curing system	15
Figure 2.5	Cross linking reaction mechanisms in the RTV-2 condensation curing of a silicone adhesive system	17
Figure 2.6	Reaction mechanisms of addition curing	18
Figure 2.7	The free radical curing reaction mechanism whereby (1) is the thermal decomposition of free radical initiator, (2) is hydrogen abstraction, and (3) is the coupling of polymer free radicals	19
Figure 2.8	The structure and bonding of different carbon allotropes – a) diamond, b) graphite, and c) fullerene	21
Figure 2.9	The three most common forms of fullerenes – a) C_{60}, b) C_{70}, and c) C_{80}	22
Figure 2.10	An example of carbon nanotube cylinder rolled up from a graphene sheet and capped at each end with hemispheres of fullerene molecule	23
Figure 2.11	Conceptualization images of SWCNTs, DWCNTs, and MWCNTs	23
Figure 2.12	The chemical structures SWCNTs rolled up from different orientation of a graphene sheet and the types of chirality of SWCNTs	25
Figure 2.13	Schematics illustrating the different strategies used to functionalize CNTs	33
Figure 2.14	The detailed procedure illustrating amino functionalization of MWCNTs - (a) addition of carboxylalkyl radicals, (b) acylation, and (c) amidation	34
Figure 2.15	Scheme for the process of grafting TETA onto the MWCNT surface	35
Figure 2.16	The crystal structure of graphite	35

Figure 2.17	Scanning electron microscope images of (a) acid-intercalated graphite, (b) expanded graphite by microwave (x50), (c) expanded graphite by microwave (x350), and (d) exfoliated graphite nanoplatelets, xGnP15	39
Figure 3.1	Chemical structure of Sylgard 182's main components: (a) Part A (dimethylsiloxane, dimethylvinyl-terminated) and (b) Part B (dimethyl, methylhydrogen siloxane)	53
Figure 3.2	(a) Representation of a typical xGnP® graphite nanoplatelets, and (b) The possible functional groups that are present in xGnP® graphite nanoplatelets	56
Figure 3.3	Overall process flow and methodology of the present research	59
Figure 3.4	A schematic of the water bath experimental set up for mixing process	62
Figure 3.5	A schematic of the mold design viewed from the top	63
Figure 3.6	Schematic on cross section of the mold configuration before cold press	63
Figure 3.7	Major parts of the DSM Micro 15 cm^3 mini extruder where a) the mixing chamber is closed and b) mixing chamber is opened	64
Figure 3.8	PDMS is pumped into the mixing chamber via feedthroat using a syringe	65
Figure 3.9	The MWCNT powder is added to the mixture through a hopper	65
Figure 3.10	Schematic of a Kapton insulated sensor with room temperature cable extension which will be connected to the hot disk machine.	69
Figure 3.11	Schematic showing the hot disk sensor fitted between two pieces of samples	69
Figure 3.12	Schematic showing the available probing depth	70
Figure 3.13	Dumbbell specimen for tension test cut according to the dimensions of Die C	71
Figure 3.14	Cross section of the copper probe used for electrical conductivity test	72
Figure 3.15	Electrical conductivity test set up	72
Figure 4.1	TEM micrographs of (a) MWCNT-p, (b) MWCNT-OH, (c) MWCNT-COOH, and (d) xGnP	78

Figure 4.2	Raman spectra of pristine MWCNT-p, MWCNT-OH, and MWCNT-COOH	80
Figure 4.3	FTIR spectrums of MWCNT-p, MWCNT-OH, MWCNT-COOH, and xGnP	82
Figure 4.4	EDS spectrums and SEM images of (a) MWCNT-p, (b) MWCNT-OH, (c) MWCNT-COOH, and (d) xGnP	84
Figure 4.5	Thermogravimetric curves for MWCNT-p, MWCNT-OH, MWCNT-COOH, and xGnP in nitrogen atmosphere	87
Figure 4.6	Transmission mode optical microscope digital images of 1 wt% pristine MWCNTs in PDMS composites produced by (a) mini-extruder and (b) solution mixing	89
Figure 4.7	SEM micrographs on fractured surface of (a) M-PDMS/1 wt% MWCNT-p, (b) M-PDMS/4 wt% MWCNT-p, (c) S-PDMS/1 wt% MWCNT-p, (d) S-PDMS/4 wt% MWCNT-p, (e) M-PDMS/1 wt% MWCNT-p, and (f) S-PDMS/1 wt% MWCNT-p. (a)-(d) were taken at 1000x magnification while (e)-(f) were taken at 5000x magnification	90
Figure 4.8	SEM micrographs of (a) M-PDMS/4 wt% MWCNT-p and (b) S-PDMS/4 wt% MWCNT-p at 10000x comparing the nanotubes length	93
Figure 4.9	Thermal conductivity of M-PDMS/MWCNT-p and S-PDMS/MWCNT-p as a function of filler loading	96
Figure 4.10	Tensile strength of composite produced by different processing methods as a function of MWCNT loading	98
Figure 4.11	Modulus at 50% elongation (M50) of composite produced by different processing methods as a function of MWCNT loading	99
Figure 4.12	Elongation at break of composite produced by different processing methods as a function of MWCNT loading	99
Figure 4.13	Electrical conductivity as a function of filler loading for composites produced by mini-extruder and solution mixing method	103
Figure 4.14	Thermogravimetric curves for composites produced by mini-extruder and solution mixing, obtained in nitrogen atmosphere. *Inset:* Enlarged curves from the range of 300 °C – 400 °C	105
Figure 4.15	CTE values of M-PDMS/MWCNT-p and S-PDMS/MWCNT-p below the T_g range	109

Figure 4.16	CTE values of M-PDMS/MWCNT-p and S-PDMS/MWCNT-p above the T_g range	110
Figure 4.17	Storage modulus as a function of temperature for composites produced by mini-extruder and solution mixing at various MWCNT-p loadings	113
Figure 4.18	Tan δ as a function of temperature for composites produced by mini-extruder and solution mixing at various MWCNT-p loadings	114
Figure 4.19	Transmission mode optical microscope images of PDMS filled with 1 wt% (a) MWCNT-p, (b) MWCNT-OH, and (c) MWCNT-COOH	116
Figure 4.20	SEM micrographs on fractured surface of (a) S-PDMS/4 wt% MWCNT-p, (b) S-PDMS/4 wt% MWCNT-OH, (c) S-PDMS/4 wt% MWCNT-COOH, and (d) S-PDMS/4 wt% xGnP, taken at 1000x magnification	118
Figure 4.21	Thermal conductivity of PDMS filled with different MWCNTs and PDMS filled with xGnP as a function of filler loading	122
Figure 4.22	Proposed chemical interaction between (a) PDMS and MWCNT-OH and (b) PDMS-MWCNT-COOH.	123
Figure 4.23	Tensile strength of PDMS filled with various fillers as a function of filler content	124
Figure 4.24	M50 of PDMS filled with various fillers as a function of filler content	125
Figure 4.25	Elongation at break of PDMS filled with various fillers as a function of filler content	125
Figure 4.26	Electrical conductivity as a function of filler loading for PDMS filled with different fillers	130
Figure 4.27	Thermogravimetric curves for composites filled with various fillers. *Inset:* Enlarged curves from the range of 300 °C – 400 °C	132
Figure 4.28	CTE below T_g and CTE above T_g for PDMS filled with 4 wt% fillers	134
Figure 4.29	Storage modulus as a function of temperature for various PDMS composites	137
Figure 4.30	Tan δ as a function of temperature for different PDMS composites	137

Figure 4.31	SEM images on fracture surface of PDMS filled with xGnP/MWCNT-OH of ratios (a) 3/1, and (b) 2/2 at 1000x magnification; (c) 3/1 at 3000x magnification	140
Figure 4.32	Schematic illustrating the formation of interconnected hybrid network between xGnP and MWCNT-OH.	142
Figure 4.33	Thermal conductivity of PDMS hybrid composites as a function of xGnP/MWCNT-OH ratio	143
Figure 4.34	Tensile properties of PDMS hybrid composites as a function xGnP/MWCNT-OH content	145
Figure 4.35	Electrical conductivity of PDMS hybrid composites as a function of xGnP/MWCNT-OH content	148
Figure 4.36	Thermal stability curve of PDMS hybrid composites. *Inset:* Enlarged curves from the range of 350 °C – 450 °C	149
Figure 4.37	T_g and coefficient of thermal expansions of PDMS hybrid composites as a function of xGnP/MWCNT-OH content	151

LIST OF ABBREVIATIONS

ASTM	American Society for Testing and Materials
CNT	Carbon nanotube
CTE	Coefficient of thermal expansion
DMA	Dynamic mechanical analysis
EDS	Energy dispersive X-ray spectroscopy
EG	Expanded graphite
FESEM	Field-emission scanning electron microscope
FTIR	Fourier transform infrared
GIC	Graphite intercalation compound
GNP	Graphite nanoplatelet
HDPE	High density polyethylene
HTV	High temperature vulcanization
LLDPE	Linear low density polyethylene
LSR	Liquid silicone rubber
M-PDMS	Composites produced by mini-extruder method
MWCNT	Multi-walled carbon nanotube
MWCNT-COOH	Carboxyl functionalized multi-walled carbon nanotube
MWCNT-OH	Hydroxyl functionalized multi-walled carbon nanotube
MWCNT-p	Pristine multi-walled carbon nanotubes
PDMS	Polydimethylsiloxane
PEI	Polyethyleneimine

PP	Polypropylene
PS	Polystyrene
RTV	Room temperature vulcanization
RTV-1	One component room temperature vulcanization
RTV-2	Two component room temperature vulcanization
SEM	Scanning electron microscope
S-PDMS	Composites produced by solution mixing method
SWCNT	Single-walled carbon nanotube
TEM	Transmission electron microscope
TGA	Thermogravimetry analysis
TMA	Thermomechanical analysis
xGnP	Exfoliated graphite nanoplatelet

LIST OF SYMBOLS

T_g	Glass transition temperature
σ	Electrical conductivity
M50	Modulus at 50% elongation
T_5	Temperature at 5% weight loss
T_{10}	Temperature at 10% weight loss
C	Carbon
O	Oxygen
Ni	Nickel
S	Sulfur
I_G	G-Band Intensity
I_D	D-Band Intensity
-COOH	Carboxyl functional group
-OH	Hydroxyl functional group
Tan δ	Loss tangent
wt%	Weight percent
vol%	Volume percent

LIST OF APPENDICES

		Page
APPENDIX A	Chemical reaction between Part A and Part B of Sylgard 182 PDMS	173
APPENDIX B	Amount of raw materials used to produce single filler composites at different filler loading	174
APPENDIX C	Amount of raw materials used to produce hybrid filler composites at different filler loading	175

KAJIAN KE ATAS PEMPROSESAN DAN SIFAT-SIFAT KOMPOSIT ELASTOMER SILIKON TERISI PENGISI KONDUKTIF TUNGGAL DAN PENGISI KONDUKTIF HIBRID

ABSTRAK

Komposit polidimetilsiloksana (PDMS) terisi nanotiub karbon dinding berbilang (MWCNT) disediakan dengan dua kaedah pemprosesan yang berbeza. Kaedah pertama melibatkan pencampuran larutan di mana MWCNT diserak dalam pelarut dengan ultrabunyi sebelum dicampur dengan PDMS secara mekanikal. Kaedah kedua melibatkan penggunaan ekstruder mini untuk menyerakkan dan mencampur MWCNT dan PDMS. Mikrograf daripada Mikroskop Imbasan Elektron (SEM) menunjukkan bahawa komposit yang disediakan dengan ekstruder mini menghasilkan nanotiub yang lebih pendek, tetapi mempunyai serakan yang lebih baik berbanding dengan komposit daripada kaedah pencampuran larutan. Komposit ini juga menunjukkan kekuatan tensil dan kekonduksian terma yang lebih tinggi. Sebaliknya, komposit daripada pencampuran larutan menunjukkan kekonduksian elektrik yang lebih tinggi dan kestabilan terma yang lebih baik. Pengfungsian nanotiub dengan –OH dan -COOH secara amnya meningkatkan kekuatan tensil, kekonduksian terma, dan kestabilan terma tetapi tidak menyumbang kepada peningkatan kekonduksian elektrik. Sifat-sifat PDMS/grafit platlet nano terkelupas (xGnP) adalah setara dengan sifat PDMS/MWCNT. Komposit terisi 4 wt% pengisi hibrid dengan nisbah xGnp/MWCNT-OH sebanyak 3/1 mempamerkan kekonduksian terma dan elektrik yang paling tinggi dan pekali pengembangan terma yang paling rendah. Secara amnya, pengisi hibrid boleh digunakan untuk menghasilkan komposit yang bersifat lebih baik pada harga yang rendah kerana kos xGnP yang murah.

STUDIES ON THE PROCESSING AND PROPERTIES OF CONDUCTIVE SINGLE FILLERS AND HYBRID FILLERS FILLED SILICONE ELASTOMER COMPOSITES

ABSTRACT

Multi-walled carbon nanotubes (MWCNTs) filled poly(dimethyl siloxane) (PDMS) composites were produced via two different processing methods. The first method is the solution mixing method where MWCNT were dispersed in a solvent using an ultrasonicator before mechanically mixed with PDMS. The second method entails the use of a mini-extruder to disperse and mix the MWCNTs and PDMS. Scanning Electron Microscopy (SEM) micrographs revealed that samples produced by mini-extruder exhibited shorter nanotubes, but better nanotubes dispersion compared with solution mixing. The composites prepared using the mini-extruder was found to have higher tensile strength and thermal conductivity. On the other hand, the composites prepared via solution mixing show higher electrical conductivity and better thermal stability. Functionalization of nanotubes with –OH and –COOH improves the tensile strength, thermal conductivity and thermal stability but does not contribute to the electrical conductivity enhancement. The properties of PDMS/exfoliated graphite nanoplatelet (xGnP) are comparable to that of PDMS/MWCNT. Composites filled with 4 wt% hybrid fillers with an xGnP/MWCNT-OH ratio of 3/1 show the highest thermal conductivity, electrical conductivity, and the lowest coefficient of thermal expansion. In general, the hybrid fillers can be used to produce composites with improved properties at lower cost due to the cheaper cost of xGnP.

CHAPTER 1

INTRODUCTION

1.1 Introduction

Silicone rubbers are found to be useful in numerous products, applications, and processes across all industries. This is because silicone rubbers possess unique physical, chemical and mechanical properties that are unmatched by any other polymeric materials. Among the properties of silicone rubbers are low surface tension, hydrophobicity, chemical resistance, electrical insulation, resistance to weathering, stability to extreme temperatures, resistance to thermal shock, high elasticity, good tear strength, capability to seal or bond materials of various natures, and so on. However, unfilled silicone rubbers usually have low mechanical, electrical and thermal conductive properties. That is why silicone rubbers are often combined with fillers such as metal powders, fumed and precipitated silica, carbon black, boron nitride and zinc oxide to improve the above-mentioned properties.

For many years, there have been extensive research on silicone rubber-based composites, for which the attentions were mostly towards the thermal properties of the materials (Sim et al., 2005; Zhou et al., 2007; Zhou et al., 2008a). With the advancement in electronics technology, miniaturization of transistors which allow more transistors to be integrated into a single device is made possible. Nevertheless, integration and cramming of transistors will increase power usage and heat flux at the device. Thus, heat dissipation issue becomes a great importance, and it is very crucial for the heat generated from the device to be dissipated as quickly and effectively as possible. Else, the operating temperatures of the device will not be

optimum, and it will reduce the lifespan of the device (Sim et al., 2005; Zhou et al., 2007; Zhou et al., 2008a).

Traditionally, to solve the heat dissipation problem, a heat sink is embedded to the device. Relying on the heat sink alone to dissipate heat is not enough due to interfacial thermal resistance arising from non-surface flatness and surface roughness of both device and heat sink. This resulted about 99% of the interfaces being separated by air gaps, which significantly reduce the capability to dissipate heat due to the poor thermal conductivity of air. Thus, an additional material, called the Thermal Interface Material (TIM) is employed between the two materials to reduce thermal contact resistance and provide effective heat conduction (Zhou et al., 2008a). There were quite a number of researches dealing with effect of fillers on the thermal conductivity of silicone rubber. Zhou et al. (2007, 2008) had reported in two separate papers that boron nitride-silicone rubber and silicon nitride-silicone rubber systems had shown a significant increase in thermal conductivity. They also reported in another paper that the thermal conductivity of silicone rubber increased with increasing alumina concentration up to 80 vol%. On the other hand, Liu et al. (2004) reported an enhancement of 65% in thermal conductivity with 4 wt% carbon nanotube (CNT) loading in silicone rubber.

Carbon nanotubes (CNTs) are new-type carbon materials that exhibit excellent mechanical properties (Yue et al., 2006). CNTs consist of folded graphene layers with cylindrical hexagonal lattice structure (Bokobza, 2008). The length of a CNT is from a few microns up to a few millimetres, with a diameter of the order of nanometers. A single carbon nanotube is hundred times stronger and six times lighter than steel and exhibits good electrical and thermal conductivities. With only a low concentration to improve the properties of the composite, it is clear that carbon

nanotube (CNTs) have attracted a great deal of interest and are the most talk about polymer composite fillers among researchers. Comparing with the enormous number of studies on the application of CNTs in epoxies, thermoplastics and fibers, there are rather few reports dealing with applications of CNTs in rubber (Das et al., 2008). Since both silicone rubbers and CNTs have their own unique and excellent properties, it is believed that combining these two groups of materials can lead to a very attractive and multifunctional composite that can find extensive application in many fields. The addition of CNTs into polydimethylsiloxane (PDMS), a type of silicone elastomer, has been reported to have improved the mechanical, electrical and thermal properties of the composites. Wu et al. (2009) reported that the elastic modulus of PDMS/CNT composite increases when 2.0 wt% CNTs are added into the PDMS matrix. Furthermore, the storage modulus and hardness also increased with the addition of CNTs. In a separate work, Hong et al. (2010b) revealed that the thermal conductivity of PDMS composite increases with filler loading.

Another emerging type of carbon-based filler is the exfoliated graphene nanoplatelets (xGnP™). Drzal's group had in recent years demonstrated that xGnP, which combined the lower price and layered structure of clays with the superior thermal and electrical properties of CNTs, can be effective alternatives to CNTs and still provide excellent and competitive functional properties (Kalaitzidou et al., 2007a; Kim and Drzal, 2009a). They also reported that the xGnP filled high density polyethylene (HDPE) composites showed superior mechanical properties while the xGnP filled linear low density polyethylene (LLDPE) displays excellence mechanical properties and electrical conductivity (Kim et al., 2009, 2010).

1.2 Problem Statement

Although previous works have shown properties improvement with the addition of CNTs in PDMS composite, the true potential of CNTs as fillers is limited and cannot be maximized because the CNTs are highly entangled (Sham and Kim, 2006). The high degree of entanglement is partly due to the high aspect ratio and high surface area of CNTs, as well as the van der Waals interactions among them. The effective use of MWCNTs in composite applications depends on the ability to disperse MWCNTs uniformly throughout the polymer matrix without reducing their aspect ratio and this issue is seen as an obstacle. This is because the dispersion of carbon nanotubes within a polymer matrix was proven to be very difficult due to the high viscosity of the polymer as well as the entanglement nature of nanotubes, which causes the nanotubes to be held together as bundles and ropes. Thus, the nanotubes have very low solubility in the polymer and tend to remain as entangled agglomerates.

Processing of CNT/polymer composites poses great challenges, primarily the non-uniform dispersion of CNTs in polymer matrix and poor interfacial adhesion between CNTs and polymer matrix (Chen et al., 2008; Yang et al., 2009). A great number of studies have been devoted in improving dispersion of CNTs in polymer matrix and interfacial adhesion between CNTs and polymers. Various processing techniques such as solution mixing (Wang et al., 2007b) and melt compounding using mini-extruder (Deng et al., 2010) were used with the intention to improve dispersion and reinforcing efficiency of CNTs in polymer. A common method to improve interfacial adhesion between CNTs and polymer matrix is by introducing functional groups on the surface of the CNTs, which can provide multiple bonding sites to the polymeric matrix (Chen et al., 2008). This can be done via treatments

using silane (Kathi et al., 2009; Zhou et al., 2008b), amine (Chen et al., 2008), fluorine (Lee, 2003) and oxidation in acid solution (Kim et al., 2005). In order to fully understand the effect of MWCNTs on the properties silicone rubber, we need to overcome this uphill challenge of preparing a composite with well dispersed nanotubes filler.

While there have been various studies on the effect of different dispersion states and parameters on the properties of CNTs polymer composites (Hong et al., 2010; Li et al., 2007; Song and Youn, 2005), minimal research has been conducted on the effect of processing methods and functionalized fillers on the properties of PDMS composites filled with MWCNTs. Besides that, very little research on the properties of exfoliated graphene nanoplatelets filled PDMS has been conducted. The current work aims to compare the properties of PDMS/MWCNT composites produced by two different methods: solution mixing and shear mixing via mini-extruder. Solution mixing is a common, low cost, and widely used method (Spitalsky et al., 2010), whereas processing of PDMS composites using mini-extruder is less common. The effect of nanotube functionalization (–OH and –COOH group) on the properties of PDMS/MWCNT composites is also investigated in the present study.

Recently, exfoliated graphite nanoplatelets have garnered a great deal of attention as promising inexpensive nanofillers and also because of their in-plane electrical, thermal, and mechanical properties which are comparable to carbon nanotubes. xGnP can be used as alternative to CNTs and still provide excellent and competitive functional properties (Kumar et al., 2010). The effect of combining CNTs and xGnPs to be used as hybrid fillers have also gained increased attention as these fillers have shown synergistic effects in enhancing the electrical and thermal conductivity of composites, especially in epoxy and polyethyleneamine (PEI)

(Kumar et al., 2010; Yang et al., 2011). However, at this time, comprehensive studies on the use of CNTs/xGnPs hybrid fillers in PDMS have not been previously reported. It is therefore believed that this work is noteworthy to produce PDMS composites with enhanced electrical and thermal conductivity while maintaining the mechanical properties at a relatively lower cost since xGnPs are cheaper than CNTs.

1.3 Research Objectives

The objectives of the present studies are as follows:

1. To compare the physical, mechanical, thermal, and electrical properties of PDMS/MWCNT composites produced by mini-extruder and solution mixing methods.
2. To study the effect of functional groups towards the physical, mechanical, thermal, and electrical properties of silicone rubber filled with MWCNT composites.
3. To compare the properties of PDMS/MWCNT and PDMS/xGnP composites and to study the properties of PDMS hybrid composites consisting of MWCNT and xGnP.

1.4 Organization of Thesis

This thesis consists of five chapters. Chapter 1 briefly introduces the properties of silicone rubber, carbon nanotubes, and exfoliated graphite nanoplatelets. A brief introduction on thermal performance challenges faced by the microelectronics industry is also described. This chapter also includes the problem

statement and objectives of the current research. Chapter 2 consists of literature review on processing of silicone rubber, carbon nanotubes, and exfoliated graphite nanoplatelets. This chapter also describes the processing of polymer composites filled with carbon nanotubes and exfoliated graphite nanoplatelets. Chapter 3 discusses the list of materials and chemicals used in this research alongside with their respective properties. The research methodology, the detailed experimental procedures to produce composites, and the methods to characterize the composites are also explained in Chapter 3. Chapter 4 discusses the results of characterization in detail, which is divided into four parts. The first part discusses the characterization of as-received fillers; the second part compares the properties of PDMS/MWCNT composites produced by mini-extruder and solution mixing method; the third part compares the properties of PDMS filled with functionalized MWCNTs and PDMS filled with exfoliated graphene nanoplatelets; the last part discusses the properties of PDMS filled with hybrid fillers. Finally, Chapter 5 summarizes and concludes the overall research. The recommendations for future studies are also listed in this chapter.

CHAPTER 2

LITERATURE REVIEW

2.1 History and Chemistry of Silicone

"Silicone" is a family of organo-silicon compounds based on a backbone or molecular chain of alternate silicon and oxygen atoms (Lynch, 1978). In addition to their links to oxygen, the silicon atoms are also bonded to organic groups such as methyl. The basic repeating unit of (R_2SiO) is known as "siloxane", where R is the organic group (Colas and Curtis, 2004). Depending on the length of the chain and the organic groups attached to the silicon atoms, these compounds can be crosslinked to form fluids, greases, gels, elastomers, and solid resins (Lynch, 1978; Rahimi and Shokrolahi, 2001).

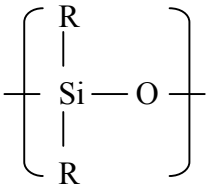

Figure 2.1: The basic repeating unit of siloxane, (R_2SiO) (Colas and Curtis, 2004).

Research on silicone chemistry started around the 1930s. In 1937, Dr. J. F. Hyde of the Corning Glass Works had developed the first practical silicone compound, a resin for used as an electrical insulating varnish. Because of its heat resistance, the resin was impregnated with glass fibers to make woven glass tapes for electrical insulation (Caprino and Macander, 1987; Lynch, 1978). In 1938, Dr.

Eugene G. Rochow began work on the methyl silicones in the General Electric Research Laboratories (Caprino and Macander, 1987). It was in 1945 that Dr. Rochow discovered the "Direct Process" for the production of chlorosilanes, which led to the economic production of silicones (Chanda and Roy, 2008; Lynch, 1978).

Silicones are derived from silica (SiO_2) or quartz, which is abundantly available in earth's crust. The production of silicone requires the silica to be reduced to silicon (Si) using an electric arc furnace. The "direct process" takes place by reacting silicon with methyl chloride in the presence of copper as catalyst (Lynch, 1978). The products of this reaction are dimethyldichlorosilane [$(CH_3)_2SiCl_2$], methyltrichlorosilane (CH_3SiCl_3), trimethylchlorosilane [$(CH_3)_3SiCl$], and a small amounts of other products. These products are separated by a large distillation tower (Caprino and Macander, 1987).

Trimethylchlorosilane is monofunctional and can be hydrolyzed to form a dimer. However, in the control of silicone polymer molecular weight, it is used as a chainstopper. Dimethyldichlorosilane is difunctional and is hydrolyzed to a mixture of linear siloxane polymers and low-molecular-weight cyclics. The hydrolyzate is then polymerized to high molecular weight with acid catalyst. Methyltrichlorosilane is trifunctional and reacts with water to form oxygen cross-linked polymers which may be used as the basis of rigid resins (Caprino and Macander, 1987; Lynch, 1978). Table 2.1 shows the basic steps in producing silicone.

Table 2.1: The basic steps in producing silicone (Lynch, 1978).

Steps	**Reaction**
1) Silica reduction to silicon	$SiO_2 + 2C \rightarrow Si + 2CO$
2) Synthesis of chlorosilanes	$Si + 2CH_3Cl \rightarrow (CH_3)_2SiCl_2 + CH_3SiCl_3 + (CH_3)_3SiCl + \ldots$
3) Hydrolisis and polymerization	*Hydrolisis of trimethylchlorosilane* $(CH_3)_3SiCl + H_2O \rightarrow (CH_3)_3SiOH + HCl$ *Polymerization of trimethylchlorosilane* 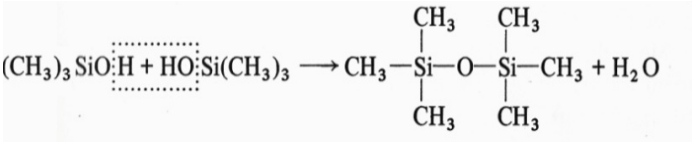 *Hydrolisis of dimethyldichlorosilane* $(CH_3)_2SiCl_2 + 2H_2O \rightarrow (CH_3)_2Si(OH)_2 + 2HCl$ *Polymerization of dimethyldichlorosilane* 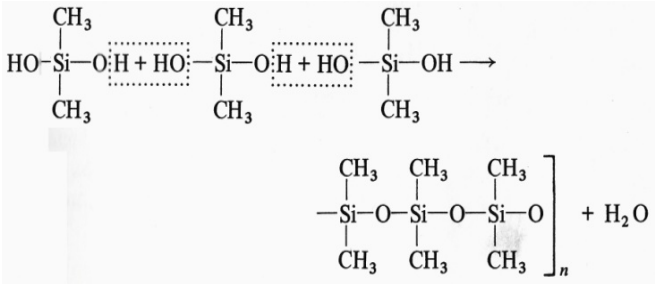 *Hydrolisis of methyltrichlorosilane* $(CH_3)SiCl_3 + 3H_2O \rightarrow (CH_3)Si(OH)_3 + 3HCl$ *Polymerization of methyltrichlorosilane* 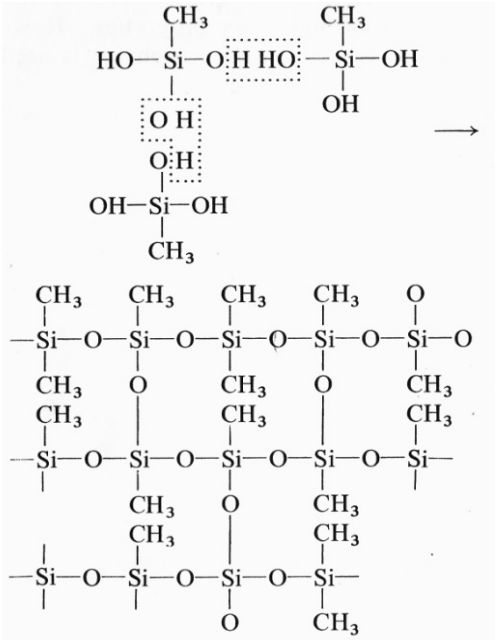

2.1.1 Silicone Elastomers

Silicone elastomers are elastic compounds which contain linear silicone polymers compounded with fillers and crosslinked in a three dimensional network. The majority of silicone elastomers contain fillers which act as a reinforcing agent or as an additive for certain mechanical, chemical or physical properties (Jerschow, 2001). Besides fillers, a typical silicone elastomer formulation contains a silicone polymer, additives, color pigments, and one or more peroxide curing agents. Although pure polymer may be used, it is generally easier and more economical to compound from silicone-reinforced gums or bases (Caprino and Macander, 1987).

Silicone elastomers are found to be useful in numerous products, applications, and processes across all industries because it possess unique physical, chemical and mechanical properties that are unmatched by any other polymeric materials (Parbhoo et al., 2002). Among the unique properties of silicone elastomers are resistance to radiation (can be exposed to radiation doses of up to 10 Mrad while losing only 25% in the maximum elongation), resistance to chemicals, high durability, resistance to weathering, good resistance to ozone and aging, resistance to thermal shocks, good tear strengths, and good electrical insulation. These unique properties have enabled the elastomers to be applied in fields as varied as aerospace, automobile, building, electronic, medical and health care, plastics, and textiles (Hofmann, 1980; Parbhoo et al., 2002).

The most outstanding characteristic of silicone elastomers, however, is the ability to maintain most of its desirable properties over the very wide temperature of -100°C to 315°C. In other words, silicone elastomers can maintain flexibility at low temperature (as low as -100°C) and also endure exposure to heat up to 315°C.

Applications which make full use of these extreme temperature characteristic are door seals and outer switch seals, which must remain flexible at low temperatures of the upper atmosphere on aerospace vehicles, or oven door seals which must withstand extremely high temperatures. Silicone elastomers inherit the outstanding high temperature properties from its strong Si-O-Si bond, which is the same bond found in quartz, sand, and glass (Hofmann, 1980; Lynch, 1978).

2.1.2 Polydimethylsiloxane

The most common known silicone is polydimethylsiloxane, abbreviated as PDMS and terminated with trymethylsiloxy (Colas and Curtis, 2004; Parbhoo et al., 2002). The chemical formula and structure of trimethylsiloxy-endblocked-PDMS are shown in Figure 2.2.

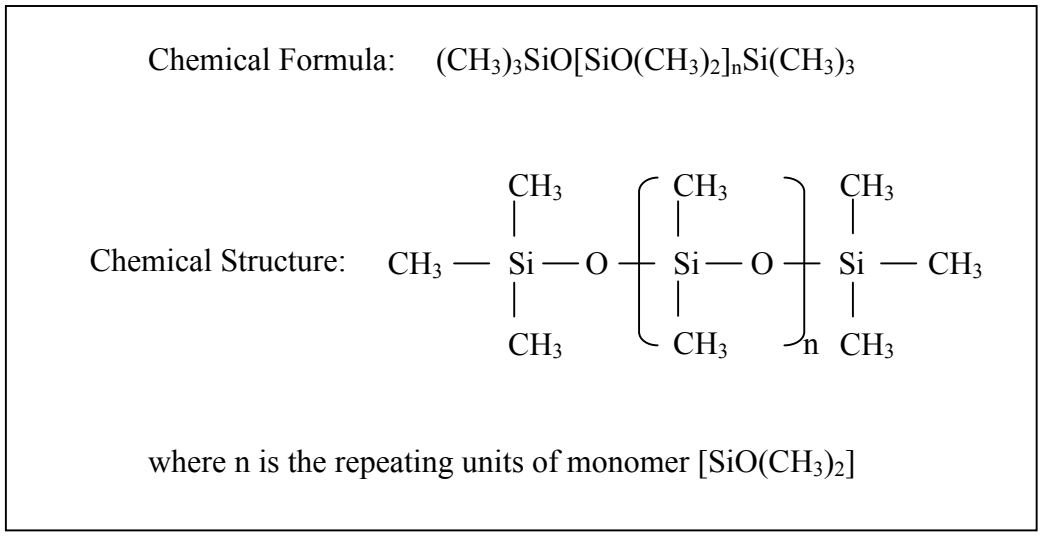

Figure 2.2: Chemical formula and structure of trimethylsiloxy-endblocked-polydimethysiloxane (Colas and Curtis, 2004).

PDMS inherits the unique properties of a silicone elastomer mentioned in section 2.1.1. Apart from those properties, other notable physical and chemical attributes in comparison to other polymers are optically clear, non-toxic, non

flammable, very low loss tangent (tan $\delta \leq 0.001$), small temperature variations of the physical constants (except thermal expansion), high dielectric strength (~14 V/μm), high gas permeability, unique flexibility (the shear modulus may vary between 100 kPa and 3 MPa), and low glass transition temperature ($T_g \approx -125°C$) (Chua, 2009; Lötters et al., 1997). The low glass transition temperature is due to the flexibility of the siloxane backbone, in addition to its large free volume and mobility (Parbhoo et al., 2002).

The production of PDMS is similar to the direct process described in Table 2.1. The first step of production is the reduction of silica to silicon, followed by synthesis of chlorosilanes from silicon. A combination of different chlorosilanes is synthesized. Dimethyldichlorosilane is separated via distillation and is then hydrolyzed to obtain disilanol that rapidly condenses to form linear siloxanes and cyclics. The linear siloxane is then polymerized and polymerization will continue until it is stopped by the addition of chainstopper or endblocking units (Colas and Curtis, 2004; Lynch, 1978).

2.2 Curing System of Silicone Elastomers

The curing system of silicone elastomers is divided into two types, namely the high temperature vulcanization (HTV) and room temperature vulcanization (RTV), depending on whether crosslinking is accomplished at ambient or room temperature. While curing is synonymous to crosslinking, the former often refers to a combination of polymerization plus crosslinking (Chanda and Roy, 2008). The room temperature vulcanization is further categorized as one-component curing (RTV-1) and two-component curing (RTV-2). Silicone elastomers are crosslinked according

to one of the following three reactions: a) free radicals, b) addition, and c) condensation (Colas and Curtis, 2004). The types of curing systems and crosslink reactions are summarized in Figure 2.3 (Jerschow, 2001).

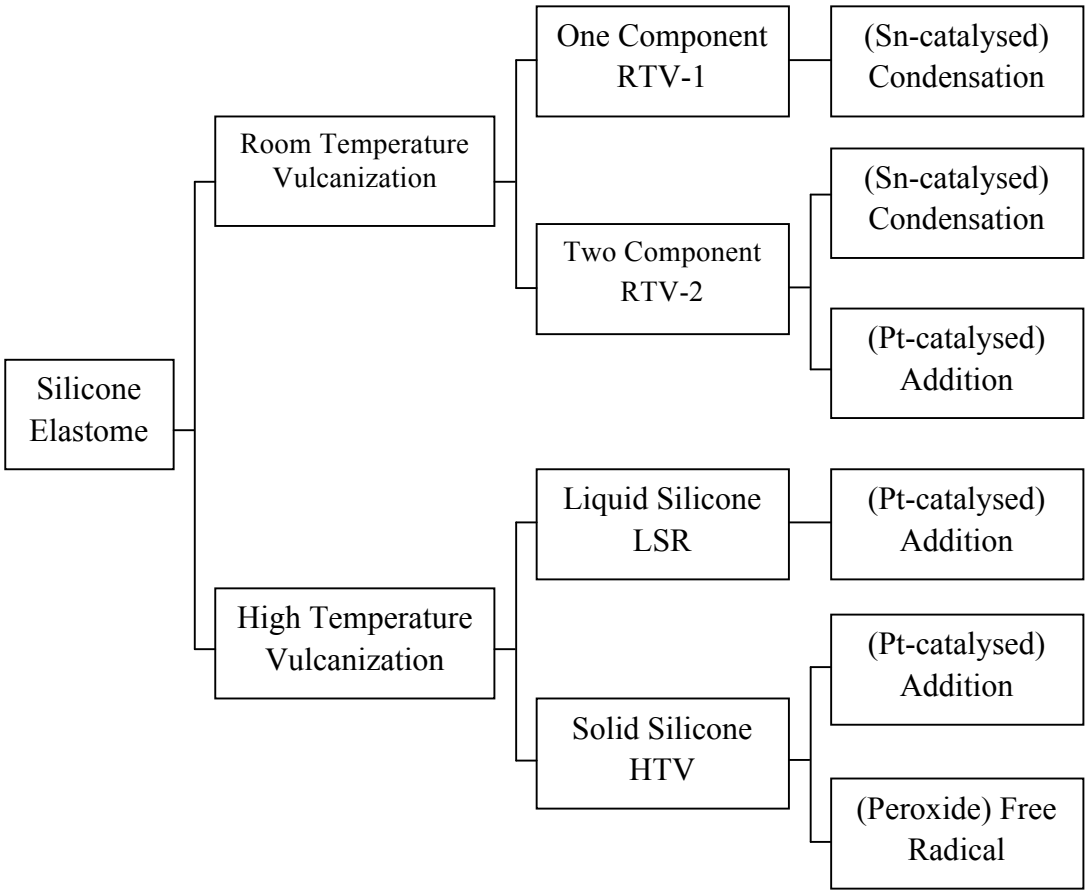

Figure 2.3: Summary of curing system and crosslinking reaction for silicone elastomer. The catalyst involved in crosslinking reaction is stated in parentheses. (Jerschow, 2001).

2.2.1 RTV-1 Condensation Curing

The one component system (RTV-1) consists of silanol-endblocked-PDMS, a reinforcing filler, a crosslinker (usually a functional silane such as methylacetoxysilane), and a tin complex catalyst (a common example is dibutyltin

laurate), all pre-blended in an air-tight package as one component (Chanda and Roy, 2008; Jerschow, 2001). In some cases, the catalyst can be either carboxylates of zinc, iron or esters of titanium. The curable composition is formed by mixing the pre-blended component in the presence of moisture. PDMS is hydrolyzed on contact of air moisture and is condensed to produce a crosslinked elastomer (Parbhoo et al., 2002).

Parbhoo et al. (2001) used a sealant cartridge as an example for application that is based on RTV-1 condensation curing. A moisture-sensitive PDMS (diacetoxymethylsiloxy-endblocked-PDMS) is prepared in situ by mixing silanol-endblocked-PDMS with triacetoxymethylsilane (crosslinker) in the catridge. Upon application of the silicone by extrusion, the silicone surface comes into with the air moisture. The acetoxy siloxy group of diacetoxymethylsiloxy-endblocked-PDMS is hydrolyzed to form a different silanol-endblocked polymer. The resulting silanol group of the polymer chain condenses with acetoxy siloxy group of another polymer chain to form a siloxane bond. This similar reaction continues until a crosslinked elastomer is produced. Figure 2.4 shows the reactions involve for the RTV-1 condensation curing system. Other application RTV-1 system is Cured-In-Place-Gasket, which is used in automotive industry to seal engine segments such as lubricating and cooling regions of the engine (Jerschow, 2001).

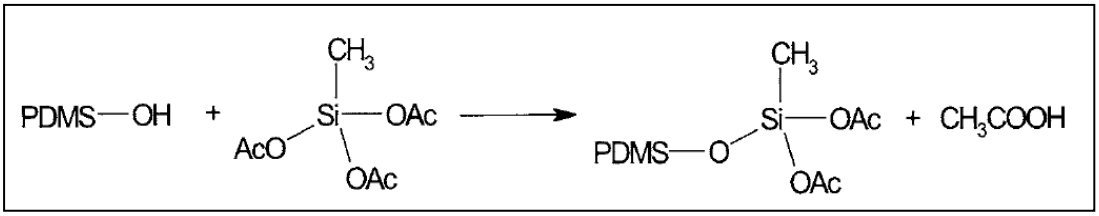

a) In situ formation of the moisture sensitive PDMS

Figure 2.4: Reaction mechanisms in the RTV-1 condensation curing system (Parbhoo et al., 2002).

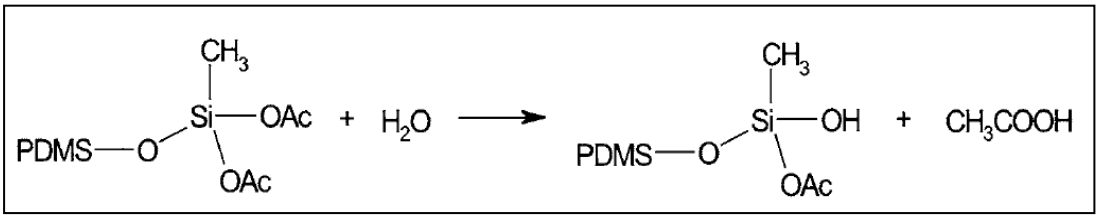

b) hydrolysis of moisture sensitive PDMS

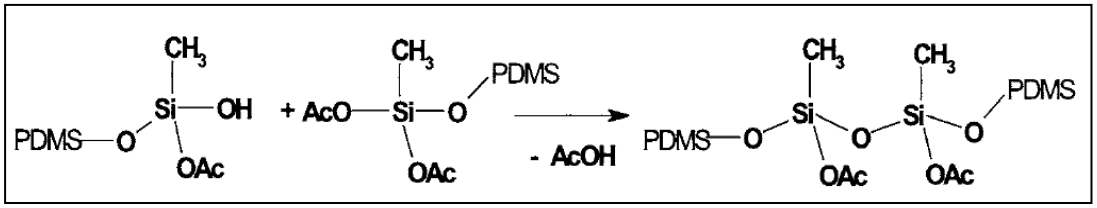

c) condensation to form siloxane bond

Figure 2.4: Reaction mechanisms in the RTV-1 condensation curing system (Parbhoo et al., 2002). *(Continued).*

2.2.2 RTV-2 Condensation Curing

As the name implies, the two component (RTV-2) condensation curing system is separated into two different components, namely the rubber base and the curing agent. The rubber base contains polymers, fillers, softeners, and additives whilst the curing agent is comprised of crosslinkers and tin catalyst, such as dibutyltindiacetate or dioctyltinmaleate (Jerschow, 2001). One major advantage of RTV-2 condensation is the moisture-sensitive catalyst is isolated from the reactive polymers prior to application. This will avoid unwanted reactions during their storage (Parbhoo et al., 2002).

When the rubber base and the curing agent are mixed together, the silanol group of the reactive polymer will condense with the alkoxy silane group of the crosslinker to form siloxane bond. The reaction is catalyzed by organo-tin compounds. The system may be cured at temperatures between 0 °C – 70 °C. At

temperature above 80 °C, the condensation reaction can be reversed and the system can revert back to a flowable polymer. The RTV-2 condensation system is cured to produce flexible elastomers that resist humidity and other hard environments, and are used in silicone adhesives, sealants, seals, and gaskets (Parbhoo et al., 2002).

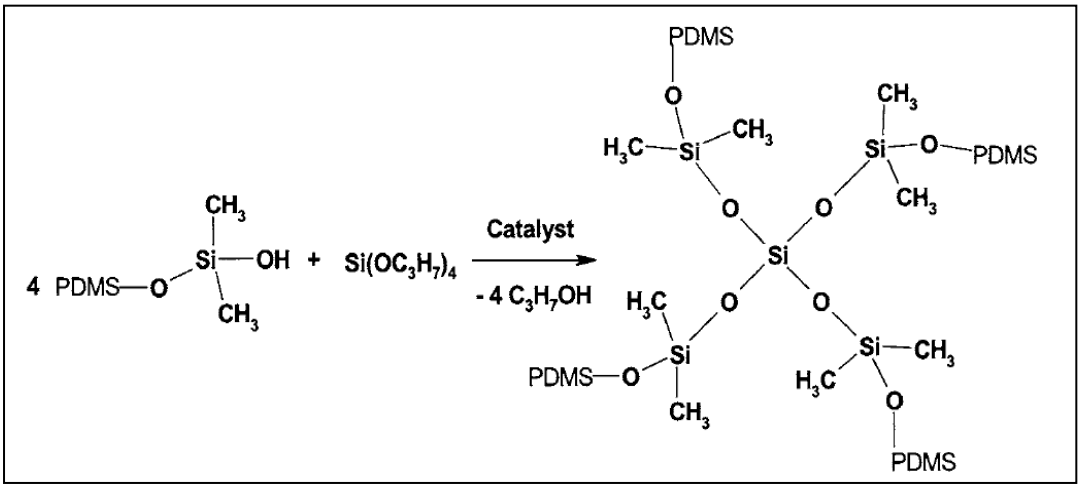

Figure 2.5: Cross linking reaction mechanisms in the RTV-2 condensation curing of a silicone adhesive system (Parbhoo et al., 2002).

2.2.3 Addition Curing

The RTV-2 addition curing system is also comprised of two different components, denoted as component A (also known as the curable composition, which contains catalyst and PDMS polymers with terminal and/or non-terminal vinyl groups) and component B (also known as the crosslinker, which contains PDMS polymer with Si-H groups). The components A and B are usually mixed according to a prescribed weight ratio (such as 1:1, 9:1, or 100:1), catalyzed by a platinum compound. Among the products of RTV-2 addition curing system are encapsulating materials, adhesives and sealants, and foam for compressible gaskets (Jerschow, 2001).

The HTV addition curing system works based on a hydrosilylation addition reaction between vinyl-functionalized and silicon-hydrido functionalized polysiloxanes. Crosslinking is achieved when the unsaturated organic groups, $CH=CH_2$ (from vinyl functionalized polysiloxanes) react with the Si-H (from silicon hydrido functionalized polysiloxanes). The reaction is catalyzed by a platinum metal complex, preferably as organometallic compound to enhance their compatibility (Colas and Curtis, 2004; Parbhoo et al., 2002).

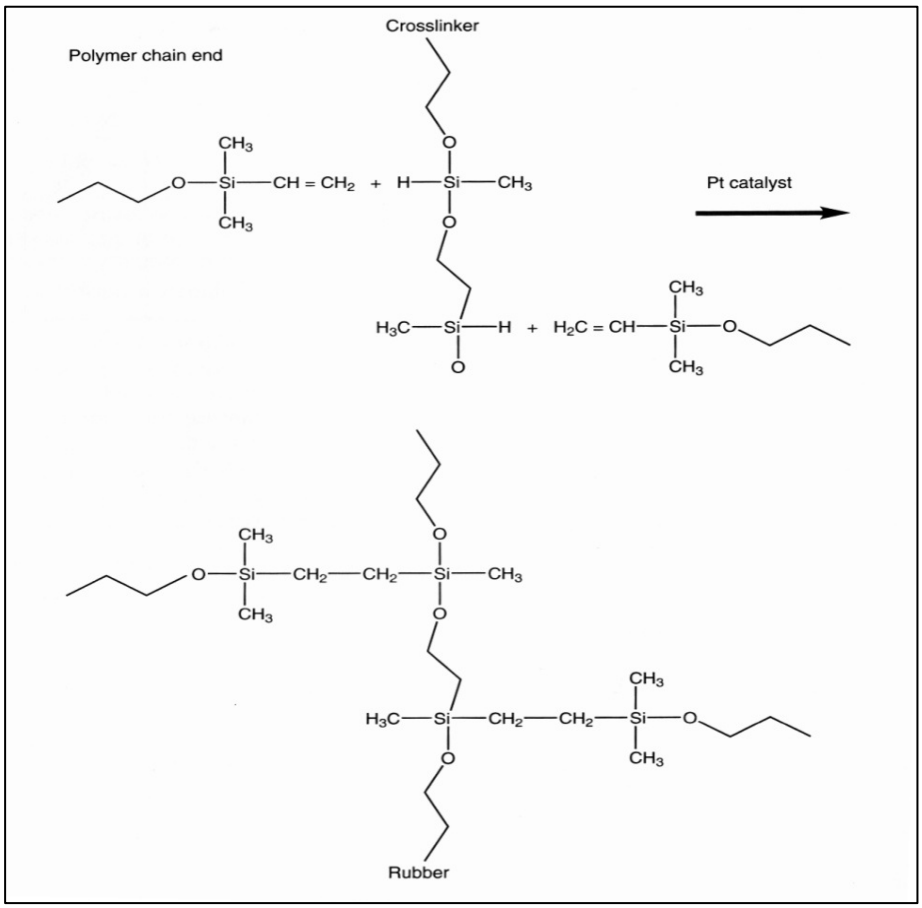

Figure 2.6: Reaction mechanisms of addition curing (Jerschow, 2001).

2.2.4 Free Radical Reaction Curing

The free radical reaction, commonly used in HTV curing, is the oldest crosslinking process used for silicones (Malczewski et al., 2003). The first step in

this process is the formation of polymer free radicals via thermal decomposition of a free radical initiator (usually organic peroxide). The polymer free radicals are obtained via hydrogen abstraction by the peroxy radicals, which is form by thermal decomposition of organic peroxide. Crosslinking is achieved by the coupling of polymer free radicals. Some common examples of organic peroxides used as free radical initiator are benzoyl peroxide, 2,4-dichlorobenzoyl peroxide, and t-butyl per-benzoate (Caprino and Macander, 1987; Chanda and Roy, 2008; Lynch, 1978).

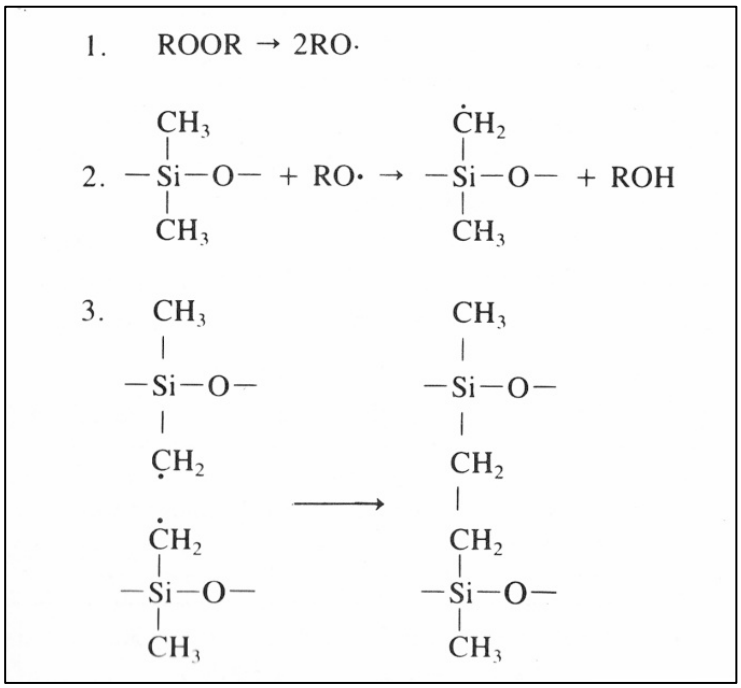

Figure 2.7: The free radical curing reaction mechanism whereby (1) is the thermal decomposition of free radical initiator, (2) is hydrogen abstraction, and (3) is the coupling of polymer free radicals (Caprino and Macander, 1987).

2.3 Introduction to Carbon

Carbon is an element with unique properties and is also the most versatile element in the periodic table. A carbon atom consists of six electrons that are shared evenly between the 1s, 2s, and 2p orbitals with an electronic ground state

configuration of $1s^2$ $2s^2$ $2p^2$ (Dresselhaus et al., 1997; Hennrich et al., 2006). The valence electrons involved in chemical bonding, occupy both the 2s and 2p orbitals. Covalent bonds are formed by promotion of the 2s electrons to one or more 2p orbitals. To achieve equal bond lengths, the 2s orbital and 2 orbitals are combined to form hybrid orbitals that are identical (Hennrich et al., 2006).

Carbon can have three different hybrid orbitals depending on the combinations involved. The first combination is between the 2s orbital and one of the 2p orbitals, resulting two sp hybrid orbitals in a linear geometry, separated by an angle of 180°. The second combination is between the 2s orbital and two 2p orbitals, resulting three sp^2 hybrid orbitals in a trigonal geometry (same plane), separated by an angle of 120°. Lastly, the third combination is between the 2s orbital and three 2p orbitals, yielding four sp^3 hybrid orbitals arranged as tetrahedron and separated by an angle of 109.5° (Hennrich et al., 2006).

Carbon can exist in three different allotropic forms, namely diamond, graphite and buckminsterfullerene. Figure 2.8 shows the structure and bonding of different carbon allotropes. Diamond has a crystalline structure where four valence electron of each carbon occupy the sp^3 hyrbid orbitals and bonds with four other carbons in a tetrahedral arrangement. This three dimensional crystalline structure makes diamond the hardest known material and gives diamond excellent thermal conduction properties. However, diamond is electrically insulating because all the electrons in diamond forms sigma (σ) covalent bonds and no delocalized pi (π) bonds (Han, 2005; Hennrich et al., 2006). In graphite, three valence electrons of each carbon occupy the planar sp^2 hybrid orbitals to form three in-plane σ bonds with an out-of-plane π bond. The result of this bonding is a hexagonal network. The

delocalized π bond is due to free movement of electrons from a non-hybrid orbital to another, forming an endless delocalized π bond network, which gives rise to the electrical conductivity (Han, 2005; Hennrich et al., 2006).

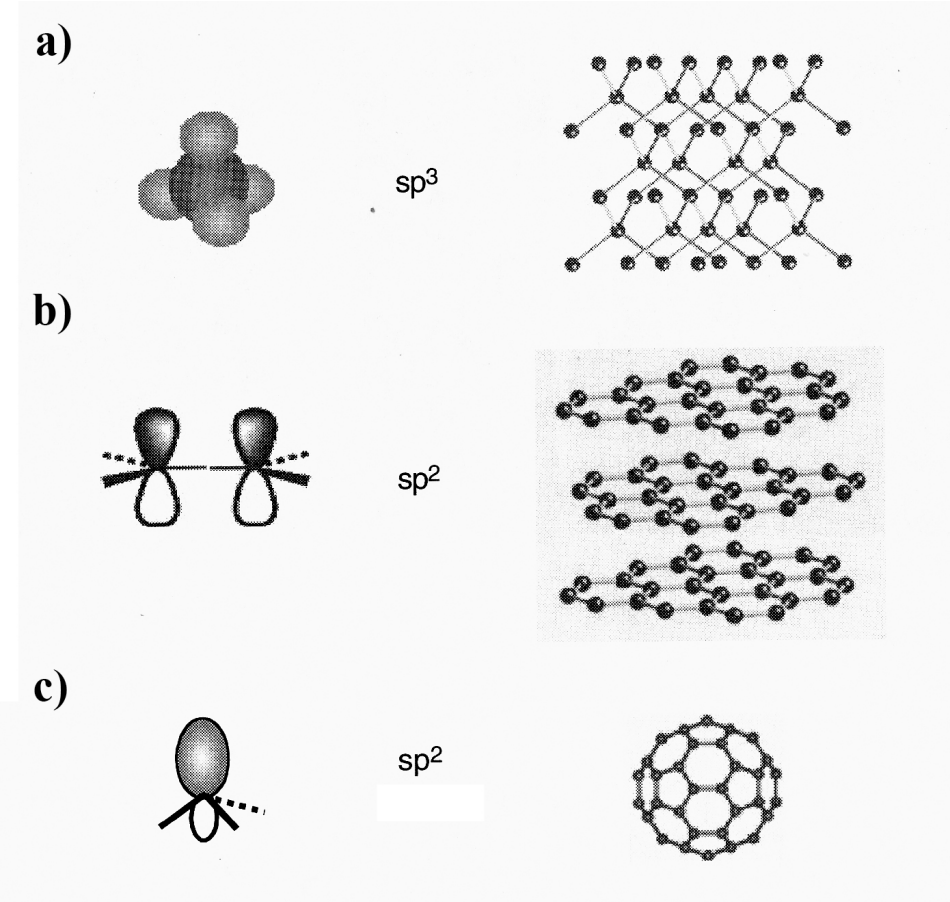

Figure 2.8: The structure and bonding of different carbon allotropes – a) diamond, b) graphite, and c) fullerene (Han, 2005).

Buckminsterfullerene, or C_{60} fullerene exists in discrete molecular form and has a hollow, cage-like spherical shape that is similar to a soccer ball. Also known as the Buckyball, each C_{60} fullerene molecule is composed of sixty carbon atoms that are bonded (sp^2) to one another to form hexagonal and pentagonal geometry configuration. There are twenty hexagons and twelve pentagons altogether (Han, 2005; Thostenson et al., 2001). Besides C_{60}, there are now more than thirty other

forms of fullerene with C_{70} being the other common fullerene (Dresselhaus et al., 1997) . Figure 2.9 shows the three most common forms of fullerenes.

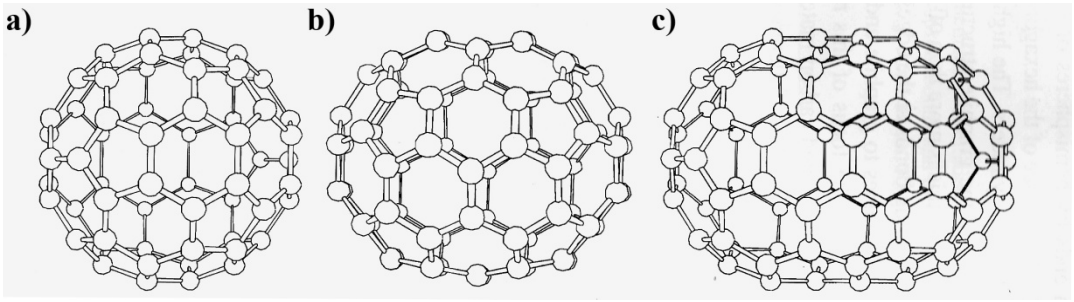

Figure 2.9: The three most common forms of fullerenes – a) C_{60}, b) C_{70}, and c) C_{80} (Dresselhaus et al., 1997).

2.4 Carbon Nanotubes

` Carbon nanotubes (CNTs) are hollow cylinders composed of one or more concentric layers of carbon atoms in a honeycomb lattice arrangement (Avouris and Wind, 2003). It is conceptualized that the cylinders are rolled from a graphene (a monolayer of sp^2-bonded carbon atoms) sheet and capped at both ends by hemispheres of fullerenes, as shown in Figure 2.10. The chemical bonding of CNTs is composed of sp^2 bonds, which is similar to those of graphite (Dresselhaus et al., 1997; Fischer, 2006). However, the carbon atoms in the cylinder display partial sp^3 character that increases as the radius of the cylinder curvature decreases (Moniruzzaman and Winey, 2006). The circular curvature will cause quantum confinement and σ-π rehybridization in which three σ bonds are slightly out of plane. To compensate this, the π orbital is more delocalized outside the tube (Han, 2005).

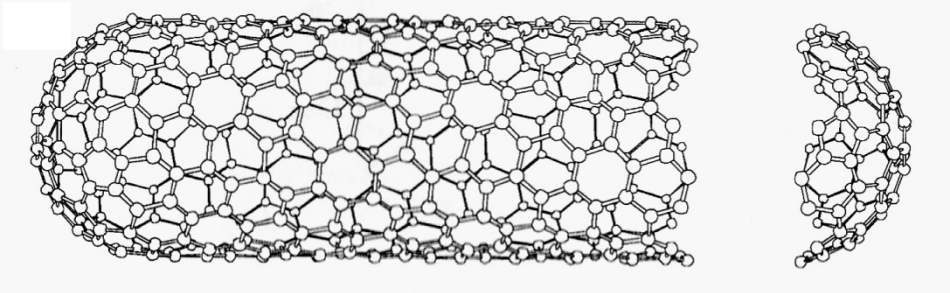

Figure 2.10: An example of carbon nanotube cylinder rolled up from a graphene sheet and capped at each end with hemispheres of fullerene molecule (Dresselhaus et al., 1997).

Depending on the structure, CNTs can be categorized as single-walled carbon nanotubes (SWCNTs) or multi-walled carbon nanotubes (MWCNTs). SWCNTs have only one layer of rolled graphene cylinder while MWCNTs consists of more than two concentric graphene cylinders. In some cases, CNTs may consist of only two layers of rolled graphne and this is known as double-walled carbon nanotubes or DWCNTs (Grobert, 2007). Figure 2.11 shows the conceptualization images of SWCNTs, DWCNTs, and MWCNTs.

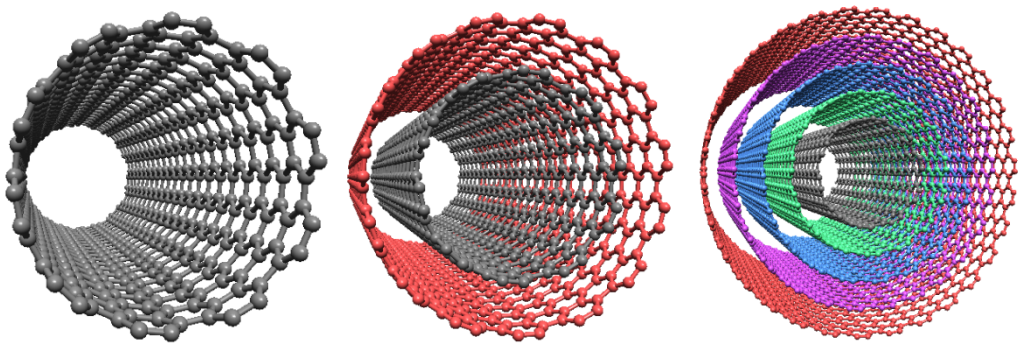

Figure 2.11: Conceptualization images of SWCNTs, DWCNTs, and MWCNTs (Shen et al., 2011).

2.4.1 Single-walled Carbon Nanotubes

` Sumio Iijima is often credited as the discoverer of CNTs although CNTs had been observed prior to his discovery (Dai, 2006; Hennrich et al., 2006). Experimental evidence of the existence of CNTs came in 1991 when multi-walled carbon nanotubes (MWCNTs) were imaged using a transmission electron microscope (Iijima, 1991). It was in 1993 that single-walled carbon nanotubes (SWCNTs) were produced by arc-discharge synthesis by two independent research groups (Bethune et al., 1993; Iijima and Ichihashi, 1993).

An SWCNT can be visualized as a one-atom-thick layer of graphene sheet rolled up into seamless cylinder of 1-10 nm in diameter and length up to several micrometers, resulting in an aspect ratio (length/diameter) larger than 1000 (Fischer, 2006). The graphene sheet may be rolled in different orientations along any two-dimensional lattice vector which then maps onto the circumference of the resulting cylinder. The orientation of the graphene lattice relative to the axis defines the chirality or helicity of the nanotube (Shaffer and Sandler, 2007).

The nanotube chirality is represented by the circumferential vector, $\boldsymbol{C_h} = n\hat{\boldsymbol{a}}_1 + m\hat{\boldsymbol{a}}_2$ and chiral angle $\theta_h = \tan^{-1}[\sqrt{3}(n/(2m + n))]$, where $\hat{\boldsymbol{a}}_1$ and $\hat{\boldsymbol{a}}_2$ are the two basis vectors of graphite and integers (n, m) are the number of steps along the unit vectors ($\hat{\boldsymbol{a}}_1$ and $\hat{\boldsymbol{a}}_2$) of the hexagonal lattice. The chiral angle is used to determine the amount of "twist" in the nanotubes and separates the SWCNTs into three chirality groups, known as armchair ($n = m$, $\theta_h = 30°$), zigzag ($n = 0$ or $m = 0$, $\theta_h = 0°$), and chiral ($0 < |m| < n$, $0 < \theta_h < 30°$) (Hennrich et al., 2006; Moniruzzaman and Winey, 2006). Figure 2.12 shows the structures of SWCNTs rolled up from a different orientation of a graphene sheet and the classification of SWCNTs based on chirality.

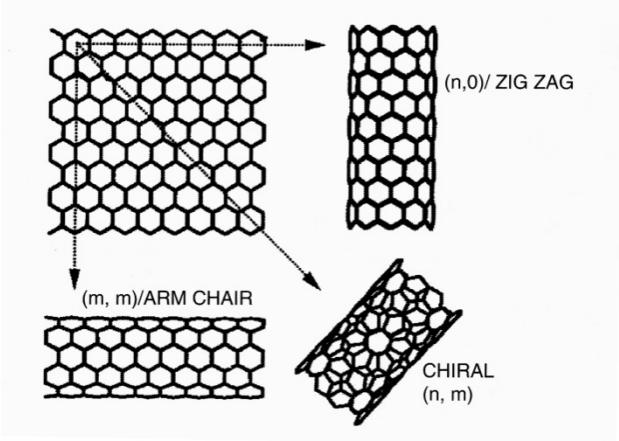

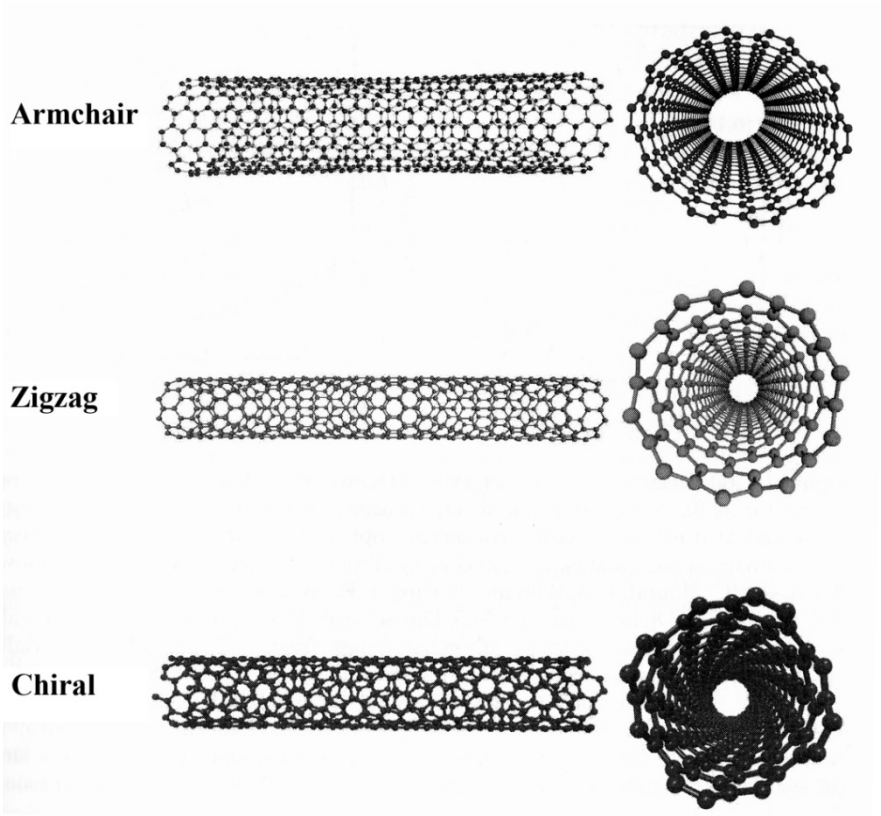

Figure 2.12: The chemical structures SWCNTs rolled up from different orientation of a graphene sheet and the types of chirality of SWCNTs (Han, 2005; Hennrich et al., 2006).

Individual SWCNT can exhibit metallic or semi-conducting behavior depending on the chirality or helicity. All armchair SWCNTs are metallic with a band gap of 0 eV while zigzag and chiral SWCNTs can be semimetals with a finite band gap if $n - m = 3i$ (i being an integer and $m \neq n$) or semiconductors with a band